batteries

MDPI

Article

On the Stability of the Interface between Li_2TiS_3 Cathode and Li_6PS_5Cl Solid State Electrolytes for Battery Applications: A DFT Study

Riccardo Rocca [1,2], Naiara Leticia Marana [1], Fabrizio Silveri [1], Maddalena D'Amore [1], Eleonora Ascrizzi [1], Mauro Francesco Sgroi [1], Nello Li Pira [2] and Anna Maria Ferrari [1,*]

[1] Chemistry Department and NIS, University of Torino, Via P. Giuria 5, 10125 Torino, Italy; riccardo.rocca@unito.it (R.R.)
[2] Centro Ricerche FIAT S.C.p.A., Strada Torino 50, 10043 Orbassano, Italy
* Correspondence: anna.ferrari@unito.it

Abstract: Lithium-titanium-sulfur cathodes have garnered interest due to their distinctive properties and potential applications in lithium-ion batteries. They present various benefits, including lower cost, enhanced safety, and greater energy density compared to the commonly used transition metal oxides. The current trend in lithium-ion batteries is to move to all-solid-state chemistries in order to improve safety and energy density. Several chemistries for solid electrolytes have been studied, tested, and characterized to evaluate the applicability in energy storage system. Among those, sulfur-based Argyrodites have been coupled with cubic rock-salt type Li_2TiS_3 electrodes. In this work, Li_2TiS_3 surfaces were investigated with DFT methods in different conditions, covering the possible configurations that can occur during the cathode usage: pristine, delithiated, and overlithiated. Interfaces were built by coupling selected Li_2TiS_3 surfaces with the most stable Argyrodite surface, as derived from a previous study, allowing us to understand the (electro)chemical compatibility between these two sulfur-based materials.

Keywords: DFT; lithium-ion batteries; solid state batteries; argyrodite; interfaces

Citation: Rocca, R.; Marana, N.L.; Silveri, F.; D'Amore, M.; Ascrizzi, E.; Sgroi, M.F.; Li Pira, N.; Ferrari, A.M. On the Stability of the Interface between Li_2TiS_3 Cathode and Li_6PS_5Cl Solid State Electrolytes for Battery Applications: A DFT Study. *Batteries* **2024**, *10*, 351. https://doi.org/10.3390/batteries10100351

Academic Editor: Karim Zaghib

Received: 18 July 2024
Revised: 2 September 2024
Accepted: 6 October 2024
Published: 7 October 2024

1. Introduction

Cathode materials for commercially available lithium-ion batteries are generally composed of transition metals (TM) oxides. A substantial portion of the employed TMs, such as Cobalt and Nickel, is categorized as critical raw material due to its high cost and the socio-economic issue related to its use. The extraction of minerals containing Cobalt and Nickel has a significant environmental and social impact, prompting research efforts to shift toward greener and less expensive materials without compromising performance. Among these alternative materials, sulfur-based cathode materials have gained traction. Lithium-rich sulfide compounds have been reported to be promising due to their high energy density and low costs. This class of compounds is composed of naturally abundant and low-cost elements, a key factor for their attractiveness, and their cyclability and safety characteristics are suitable for the application as lithium-ion battery (LIB) cathode materials. The lithium-titanium-sulfur family of compounds has been studied and investigated from different points of view. Among all possible structures and stoichiometries, disordered cubic rock-salt type Li_2TiS_3 showed interesting features and performances. It is reported that, compared to its iso-stoichiometric layered structure, rock-salt type Li_2TiS_3 is characterized by a higher capacity—over 400 mAh·g^{-1} in a voltage window between 1.5 and 3 V vs. Li^+/Li [1,2]. The performance characteristics of this material have been studied with the employment of DFT methodologies by Sakuda et al. [3–5] and by our research group [6,7]. A thorough evaluation of its properties was performed: crystal structures, spectroscopic, and electronic properties were analyzed to elucidate the most

stable structures and configurations. Furthermore, we explored the structural evolution and relative variations in properties in relation to cycling processes. Our previous efforts helped us to fully comprehend the system, this knowledge being essential to perform more challenging simulations.

The described cathode material is well-suited for application in all-solid-state cells, also known as Gen4 cells. This class of cells employs solid electrolytes (SE) in place of liquid or gel electrolytes [8], presenting numerous potential advantages: enhanced safety, increased energy density, long-term stability and cycle life, reduced size and weight, and the capability to tolerate fast charging. Recently, numerous sulfur-based compounds with superionic conductivities have been proposed, and this has aroused great interest because of their potential applications. Due to their nature and chemical composition, this class of compounds can provide good chemical compatibility and an easy coupling with sulfur-based cathodes. Among sulfur-based solid electrolytes, Argyrodites, specifically Li_6PS_5X with X = (Cl, Br, I), are a class of materials renowned for their unusually high Li^+ mobility [9,10]. Within this category, Li_6PS_5Cl has received significant attention due to its distinctive characteristics, such as the very high conductibility (10^{-3} S cm^{-1}) [11,12]. The study of its structure, thermal and mechanical stability, and electronic properties has been the subject of a previous publication by some of us [9].

In this work, our goal is to build up cathode/SE interfaces by combining the most stable surface of LTS, selected from the surfaces analyzed herein, with the most suitable surfaces of Argyrodite. The selection is grounded on criteria based both on the chemical compatibility deduced from the morphology of the involved surfaces and on the need to build junctions with minimal mechanical stress. To simulate battery operating conditions during cycling, involving delithiation processes in the cathode, one heterostructure with a partially delithiated LTS surface was analyzed to assess the impact of delithiation on the chemical stability of the interface. Furthermore, since LTS was found to accommodate additional Li atoms up to a $Li_{2.23}TiS_3$ stoichiometry [3,13], a partially overlithiated structure was also considered. The selected heterostructures were extensively evaluated and analyzed to include morphology, electronic structure, chemical stability, and potential mechanical issues.

Despite the inherently idealized nature of the proposed model of heterojunctions in half-batteries, we believe that the comprehensive analysis performed in this study, aimed at deepening our understanding of the properties of these systems, can be valuable for assessing their suitability in real LIB. This knowledge contributes to the further advancement of sustainable and efficient lithium-ion battery technologies.

2. Computational Methods

Calculations were performed employing the most recent version of the CRYSTAL program [14], based on DFT Hamiltonians and PBE0 hybrid functional [15,16]. All-electron basis sets 6–11 G, [17] 86–311 G*, [18] 85–211 dG, [19] were used to describe Li, S, and P atoms, while a Hay–Wadt small core pseudopotentials [20] (12 electrons) together with 4111-31 (4sp,2d) contracted GTFs were used for Ti atoms. The adopted computational scheme, as reported in [21], produced accurate results in our previous studies on comparable systems [6,9,22]. To improve the estimation of noncovalent interactions involved in interface formation, energy evaluations were carried out using the Minnesota hybrid functional (MN15) [23] through single-point energy calculations based on PBE0 optimized structures.

To control the truncation criteria for the bi-electronic integrals, the five thresholds employed were [7, 7, 7, 7, 14]. The shrinking factor in reciprocal space, as well as for a denser k-point grid, was set to 3 for the surface simulations and the interfaces, which correspond to 5 independent k-points in the irreducible part of the Brillouin zone.

In the CRYSTAL code, surfaces are represented as periodic slab models with infinite dimensions along the x and y axes and a finite thickness in the z axis. Li_2TiS_3 (LTS) surface optimizations were performed with the lattice parameters fixed at their bulk values, and the same approach was applied for optimizing the heterostructure.

The structural stability of the surfaces was assessed based on the surface energy (E_{surf}), calculated as:

$$E_{surf} = \frac{E_{slab} - nE_{bulk}}{2S} \quad (1)$$

where E_{slab} and E_{bulk} are the optimized energies of the surface and bulk, respectively, n represents the number of LTS units in the slab structure, and S is the surface area.

The LTS/Argyrodite interfaces were modeled by taking into account the most stable surface of Argyrodite, the (001) [9], and the LTS surfaces. The structural stability of these interfaces was determined by evaluating the corresponding adhesion energy per unit surface area, E_{adh}, computed as:

$$E_{adh} = \frac{E_{LTS/Argy} - (E_{LTS} + E_{Argy})}{S} \quad (2)$$

$E_{LTS/Argy}$, E_{LTS}, and E_{Argy} are the total energy of the optimized interface, and the isolated LTS and Argyrodite surfaces, respectively. The LTS surface was kept fixed at the bulk lattice parameters, defining the lattice parameters of the interface, while the Argyrodite surface was structurally adjusted to align with the substrate. The strain energy is defined by the energy cost for this deformation (per surface unit), E_{strain}, which have to be considered for a correct estimate of the total stability of the composite. E_{strain} was computed as:

$$E_{strain} = \frac{E_{Argy\_LTS} - nE_{Argy\_fullopt}}{2S} \quad (3)$$

$E_{Argy\_fullopt}$ represent the energy of the fully relaxed Argyrodite surface, while E_{Argy_LTS} denotes the energy of the overlayer Argyrodite optimized at the lattice constants of the substrate LTS.

The Basis set Superposition Error (BSSE) was estimated a posteriori, by applying the standard counterpoise method [24].

3. Results and Discussion

3.1. Li_6PS_5Cl and LTS Surfaces

3.1.1. Li_6PS_5Cl

In a previous paper, we reported the 2D slab models for pseudo-cubic structures of Argyrodite [8] in terms of surface stability and how they influenced the Argyrodite crystal formation. Argyrodite is an insulator, or rather a wide gag semiconductor, with a band gap (E_G) of 3.63 eV (calculated at PBE0 level). However, the outstanding ionic conductivity properties are related to its structural characteristics, such as lithium content, vacancies, and structural channels, rather than the size of the band gap, and it can be successfully applied as a superionic solid electrolyte in a lithium solid-state battery, as widely reported in literature (see, for instance, Ref. [25]). According to our calculations, the most stable surfaces are (111), (001), and (110), with surface energy values of 18.54 meV/Å^2, 21.47 meV/Å^2, and 18.16 meV/Å^2, respectively. The (111) and (001) slabs are not symmetric, i.e., the top and bottom terminations are different, while the (110) is symmetric, and its terminations are predominantly composed of tetrahedral [PS_4] clusters. The (001) surface presents the most interesting structure, with a well-defined Li_2S layer at one termination (see Figure 1), a passivating material that can act as a barrier against further decomposition of the alkali superionic conductor electrolyte [26,27]. Furthermore, its lattice parameters of a = 7.06 Å and b = 6.90 Å are the closest to the lattice parameters of the LTS surface, which could generate an interface with small strain, leading to better adhesion, as will be discussed later. For the mentioned reasons, we chose to exclusively focus on the (001) surface of Argyrodite, as it best suits the scope of the paper of identifying stable interfaces.

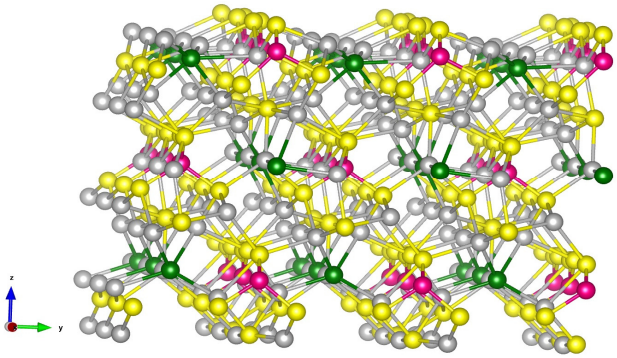

Figure 1. (001) Argyrodite surface. The yellow, gray, green, and magenta spheres represent the sulfur, lithium, chlorine, and phosphorus atoms.

3.1.2. Li_2TiS_3 (LTS)

In our previous investigation [6,7], we introduced and thoroughly analyzed the bulk structure of LTS. For this purpose, we utilized a primitive cell consisting of 54 atoms, including 18 Li, 9 Ti, and 27 S, maintaining the stoichiometry of Li_2TiS_3. Our results revealed that structures with a more uniform dispersion of titanium atoms, where titanium atoms were evenly distributed within the Li sublattice, demonstrated improved stability. The proposed configuration for Li_2TiS_3 indeed manifested as a pseudo-cubic structure, with titanium dispersed throughout the lattice and no observable signs of internal clusterization. The most stable pseudo-cubic Li_2TiS_3 structure is characterized by a = 15.22, b = 15.27, c = 15.22 and $\alpha = 90.2°$, $\beta = 89.9°$, and $\gamma = 90.2°$, with Li–S that ranges from 2.49 to 2.99 Å and Ti–S that ranges from 2.22 to 3.30 Å, with E_G = 2.72 eV.

Low Miller index surfaces (100), (110), and (111) have been cut from the bulk, and representative stoichiometric two-dimensional slabs are sketched in Figure 2. The (111) surface is a polar one as it alternates planes containing only S anions or only Ti and Li cations. In this work, we do not consider matter displacement or the introduction of non-stoichiometric defects; therefore, the charge compensation needed to avoid the Coulomb catastrophe occurs self consistently, with the metallization of the surface. For this reason, this surface will not be considered anymore.

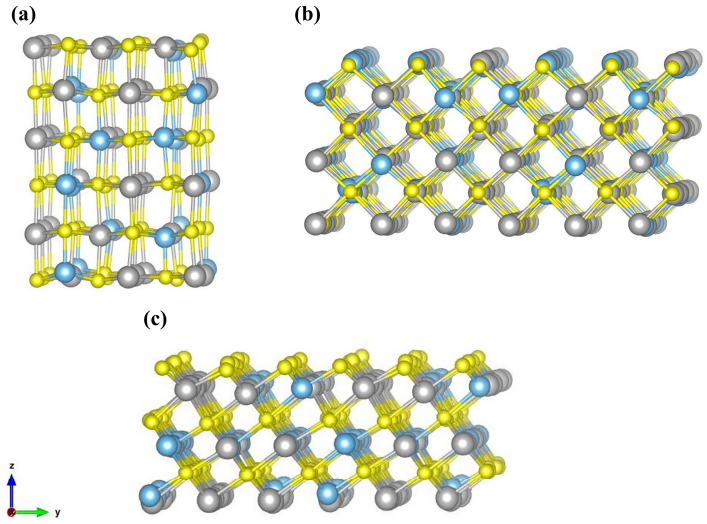

Figure 2. Schematic representation of LTS surfaces (**a**) (100), (**b**) (110), (**c**) (111). Yellow, gray, and light blue spheres refer to sulfur, lithium, and titanium atoms, respectively.

Let us now examine the (100) surface. Due to the uniform dispersion of Ti ions within the Li-ion sublattice, each layer obtained from slabs cut along this direction appears

stoichiometric and electrically neutral. Slabs with thicknesses of 5, 7, and 13 layers have been considered and relevant properties are reported in Table 1.

Table 1. LTS surfaces structural properties. The number of layers of each slab, $n_{layer,}$ surface z-thickness (in Å), (Li–Li) bond length of inner layers, d_{inner} (in Å), Li–In (Li–Li) bond length of the outer layers, d_{outer} (in Å), surface energy (E_{surf}, in meV/Å^2), and the band gap (E_G, in eV) are reported.

LTS	n_{layer}	*z*-Thickness	d_{inner}	d_{outer}	E_{surf}	E_G
(100)	5	10.5	2.59	2.48	20.85	2.87
(100)	7	15.3	2.54	2.46	22.60	2.81
(100)	13	30.6	2.54	2.46	22.52	2.74
(110)	6	8.9	1.78–1.88	1.70–1.72	43.40	1.17
(110)	12	19.7	1.80–1.85	1.70–1.74	44.30	1.46

As expected, the surface exhibits significant relaxation, evident by considering the interlayer spacing, d, which has been calculated based on the average z position, z_{ave}, of all ions in each plane. Indeed, d of the terminal layers, d_{outer} = 2.46 Å, is notably reduced compared to the corresponding values of the internal layers, d_{inner} = 2.54 Å. The shrinkage of d_{outer} is well-known to stem from electrostatic effects due to the undercoordination of the ions in the outer layer. It is the result of a remarkable downshift of the outermost cations that is particularly pronounced for Ti due to its larger formal charge (0.05 Å for Li and 0.24 Å for Ti, computed with respect z_{ave} of the plane) despite a significant rumpling of sulfur ions, upshifted by 0.11 Å.

E_{surf} is relatively low, around 22 meV/Å^2, indicating a high level of stability for this surface. Considering the different terminations that these slabs typically exhibit, the calculated E_{surf} represent an average value between these terminations. Furthermore, the difference between the values obtained for 5-layer and 7–13-layer slabs is only 0.02 meV/Å^2. This slight difference indicates that a 5-layer slab is already adequate and can be confidently used to represent the surface.

In the (110) surface, the cut along this direction does not ensure stoichiometric and electrically neutral layers. To fulfill these requirements, one must consider a slab with a thickness of six layers (or its multiples). This is essential because, in this case, the number of atoms in the surface cell is 108, corresponding to twice the number of atoms in the bulk primitive cell, thus ensuring stoichiometry and electroneutrality. For this surface, we specifically considered 6- and 12-layer slabs and their relevant properties are detailed in Table 1.

Significant relaxation also occurs for this surface, since d_{outer} is remarkably smaller than d_{inner}, but with more variability than seen in the (100) surface due to the different number of cations and anions in each individual layer. The calculated value for E_{surf} of (110) is twice as large as that calculated for the (100) surface (see Table 1). This increase of E_{surf} primarily results from the exposed ions having a four-coordination, compared to the five-coordination observed in the (100) surface, which decisively contributes to the reduced stability of the surface.

The ideal Wulff crystal, derived from the surface energies listed in Table 1, exclusively exhibits the (100) surface (see Figure S3). The crystal shape begins to change, with a very slight exposure of the (110) surface, only when the surface energy of the (110) surface is hypothetically reduced by 30% (from ~44 to ~30 meV/Å^2). For these reasons, we chose to focus exclusively on the (100) surface for the remainder of the study, as it shows significantly higher stability compared to other LTS low-index surfaces, making it the most relevant for constructing realistic interfaces with this material.

When attempting to pair a solid electrolyte with a positive cathode, it is crucial to verify the electrochemical stability of the junction. The energy levels of the solid electrolyte and electrodes provide us with information about the electrochemical window (which limits the cell's open-circuit voltage) and also assist in predicting the theoretical chemical stability

of the electrolyte/electrode system. The chemical potential for the cathode semiconductor, $\mu_{cathode}$, is described by the bottom of the conducting band (BCB). If $\mu_{cathode}$ is below the top of the valence band (TVB) of the electrolyte the latter can be oxidized, unless the reaction is obstructed by a passivating layer. In the present case, theoretical chemical stability is predicted by comparing the electronic levels of the TVB of Argyrodite and the BCB of LTS, as derived by the PDOS of Figures S1 and S2 in the Supplementary Material. The BCB position of LTS is significantly higher (2.52 eV) than the TVB of Argyrodite, indicating the stability of the electrolyte with respect to oxidation and thereby ensuring the chemical stability of the interface. The difference between the TVB of the solid electrolyte and the BCB of the cathode is defined as ΔE and used as indicator of the oxidizing power of the electrode towards the electrolyte, as can be inferred by analyzing the separate components of the heterojunction. The ΔE value for this heterojunction is schematically reported in Figure 3a. The energy levels are referred to the vacuum level, which the CRYSTAL code, dealing with real 2D systems, correctly computes as the zero value of the electrostatic potential.

Understanding the stability of the junction also requires examining how the battery performs under different lithium content. When the cathode undergoes the delithiation process (during the charging cycle), sulfur oxidation from S^{2-}--S^{2-} to $(S–S)^{2-}$ begins, with the formation of sulfur bridges. Evidence of this phenomenon can be found in the literature [3] and in our previous study [7], where every removal of two Li atoms leads to the formation of one $(S–S)^{2-}$ bridge. If an odd number of Li atoms is removed, a single electron leaves the structure, causing partial S oxidation through the formation of an electron vacancy localized on one or more S^{2-} atoms nearby the newly formed vacancy.

In this work, we selected two delithiation states that corresponds to a delithiation of 44% and 50%, obtained by removing 8 and 9 lithium atoms from the primitive cell, named, respectively, LTS_{even} and LTS_{odd}, as they correspond to supercell of structures with even and odd delithiation numbers, respectively. All delithiation sites were selected according to the structures reported in our previous work [7]. In the 5-layer slab representing the (100) delithiated surfaces, the LTS_{even} structure corresponds to an overall removal of 32 Li atoms, creating 16 sulfur bridges; in the case of the LTS_{odd} structure, 36 Li atoms are removed, leading to the formation of 16 sulfur bridges and 4 electron vacancy localized on four or more S atoms. Such an atomic arrangement can describe the situation of odd delithiation in a redundant way or the initial stage of the transient process that, from a partial oxidation of isolated S^{2-} atoms, lead to complete oxidation to form $(S–S)^{2-}$ bridge. The presence of $(S–S)^{2-}$ bridge structural units lead to cell expansion (up to 130%) and a gradual loss of crystallinity, as detailed in [7]. From the perspective of the electronic structure, the most significant aspect of the oxidation of S^{2-} is an upward shift of the S 3sp states of the valence band (VB), leading to a contraction of the band gap from 2.88 eV in pristine LTS to 2.60 eV and 2.69 eV in LTS_{even} and LTS_{odd}, respectively (see PDOS reported in Figure S1 of Supplementary Materials).

Moreover, LTS can accommodate a certain percentage of extra lithium atoms in the crystalline structure; this non-stoichiometric Li insertion is energetically favored. In our previous work [7], we demonstrated that the extra Li is interstitially hosted in tetrahedron sites, preferentially surrounded by other Li cations. In this work, we selected a surface with 3% extra Li atoms inserted. Overlithiation causes Ti^{4+} reduction to Ti^{3+} for charge compensation; Ti^{3+} states affect both the valence and the conduction bands, determining a significant decrease of E_G to 2.29 eV, see Figure S2.

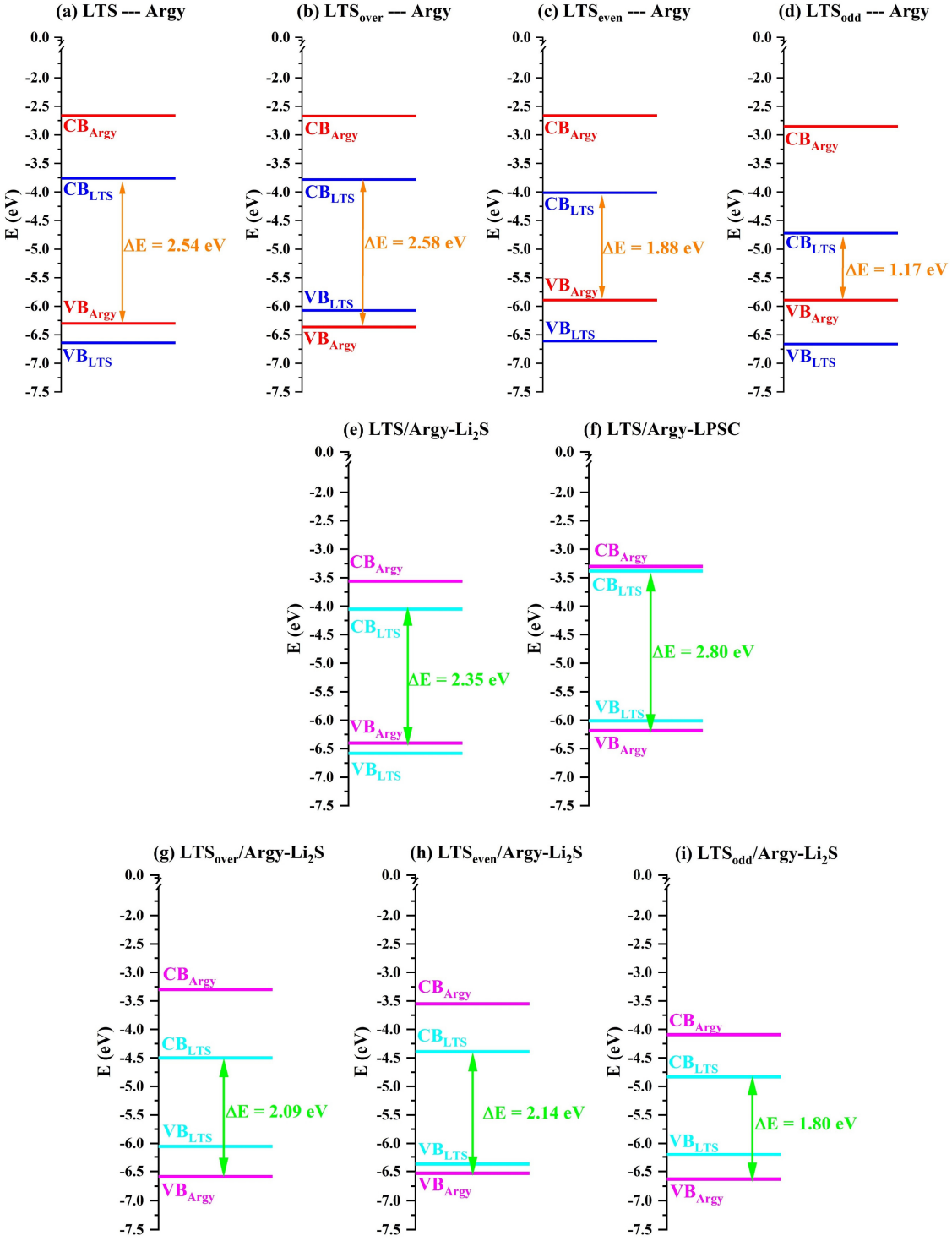

Figure 3. Comparison between the bottom of the conducting band (BCB) and the top of the valence band (TVB) levels for the (**a**–**d**) isolated LTS and Argyrodite surfaces, and (**e**–**i**) formed interfaces for different LTS lithium content and the two Argyrodite terminations. The lines in blue, red, cyan, and magenta represent the energetic level of pristine LTS and Argyrodite surfaces, and the same surfaces on the formed interfaces, respectively.

The ΔE of LTS$_{even}$, LTS$_{odd}$, and LTS$_{over}$ are 1.88, 1.17 eV, and 2.58 eV, respectively, to be compared with the value of 2.46 eV for pristine LTS, as shown in Figure 3b–d. Although the ΔE values remain positive, indicating a general difficulty in oxidizing the electrolyte, they also show a significant dependence on the degree of delithiation of LTS.

However, assessing the (in)stability of the electrode/electrolyte interface is complex and cannot be determined solely by the alignment of energy levels of separate components. Therefore, explicit models of the interface must be investigated to obtain a more detailed and realistic picture. The following paragraph presents and analyzes the structures of LTS/Li_6PS_5Cl interfaces.

3.2. LTS/Li_6PS_5Cl Interfaces

To build a stable and chemically sensible (100)LTS/(001)Li_6PS_5Cl heterostructure (hereafter referred to as LTS/Argy), it is crucial to identify a suitable coincidence cell between these materials. This approach aims to maximize adhesion energy and minimize strain. Key considerations include: (i) Chemical compatibility: preserving the integrity of the pristine structures while facilitating the formation of new chemical bonds at the interface ensures heterostructure stability; (ii) Mechanical issues: significant lattice parameter mismatch between the substrate (LTS) and overlayer (Li_6PS_5Cl) can induce strain sufficient to destabilize the structure. Therefore, choosing the interface coincidence cell involves striking a necessary balance between model accuracy and computational feasibility.

To attend to all the requirements described above, a (2 × 2) supercell of (100) Li_2TiS_3 surface was combined with a (3 × 3) supercell of (001) Li_6PS_5Cl surface, resulting in an interface composed of 711 atoms with lattice parameters a = 21.54 Å and b = 21.59Å. The (001) Argyrodite surface has two different terminations [9]: one which exposes a layer of Li_2S to the vacuum, and the other showing a mixed LiCl and PS_4 layer; we named the two terminations as Argy-Li_2S and Argy-LPSC. As a result, two different interfaces were investigated, LTS/Argy-Li_2S and LTS/Argy-LPSC. The two optimized interfaces are reported in Figure 4, and their main properties are summarized in Tables 2 and 3. The small strain energy value (3.03 meV $Å^{-2}$ for both terminations), indicates that Argyrodite suffers negligible tensile strain when matching to the LTS surface.

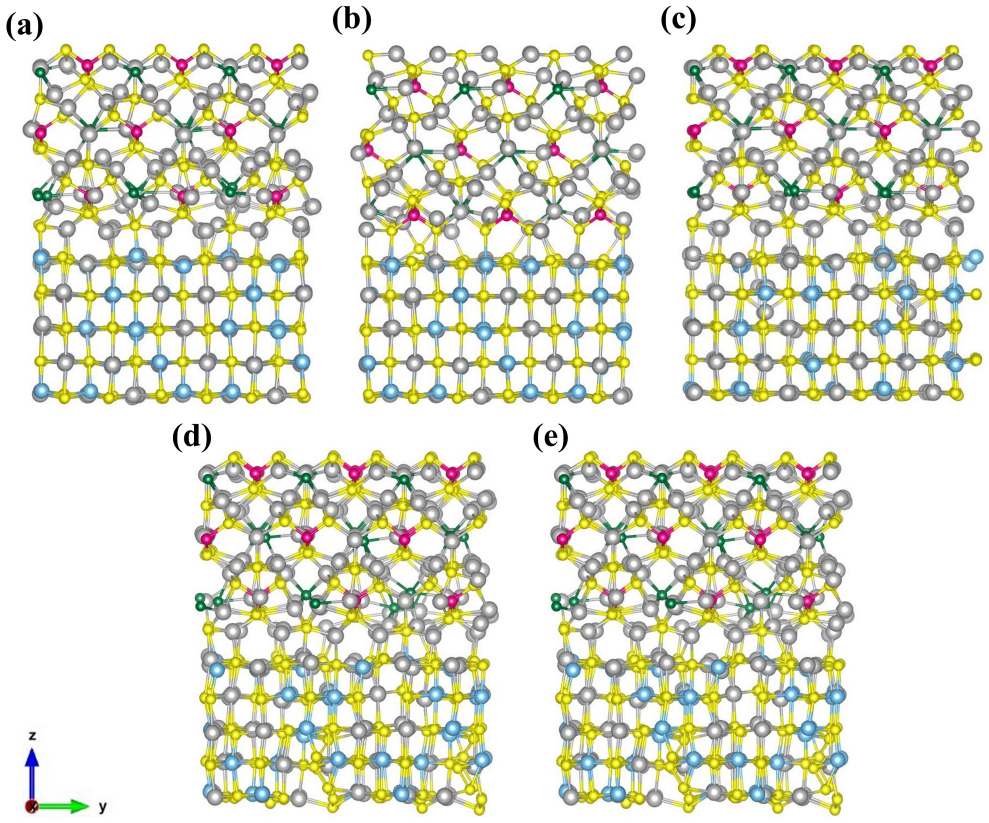

Figure 4. Final optimized (100)LTS/(001)Argy interfaces (**a**) LTS/Argy-Li_2S, (**b**) LTS/Argy-LPSC, (**c**) LTS_{over}/Argy-Li_2S, (**d**) LTS_{even}/Argy-Li_2S, and (**e**) LTS_{odd}/Argy-Li_2S. The yellow, gray, light blue, green, and magenta spheres represent the sulfur, lithium, titanium, chlorine, and phosphorus atoms.

Table 2. Lattice parameters (a and b, in Å) and mismatch (a% and b%) for the four LTS/Argy. The Argy lattice parameters are reported as a reference.

Interface	a	a%	b	b%
Argy	21.16		20.72	
LTS/Argy	21.54	1.73	21.59	4.21
LTS_{even}/Argy	22.38	5.77	22.38	8.04
LTS_{odd}/Argy	22.38	5.77	22.38	8.04
LTS_{over}/Argy	21.77	2.89	21.79	5.20

Table 3. Structural properties computed with different functionals for the four different LTS/Argy interfaces. Adhesion energy (E_{adh}), strain (E_{strain}), basis set superposition error (E_{BSSE}), BSSE corrected adhesion energy (E^c_{adh}), in meVÅ^{-2}, and electron charge transfer from Argy to LTS (CT, in 10^{-3} | e | Å^{-2}) for the analyzed interfaces are presented.

Functional	Interface	E_{adh}	E_{strain}	E_{BSSE}	E^c_{adh}	CT
PBE0	LTS/Argy-Li_2S	−25.32	+3.03	+3.71	−21.62	1.147
PBE0	LTS/Argy-LPSC	−9.18	+3.03	+3.06	−6.12	0.724
MN15//PBE0	LTS/Argy-Li_2S	−35.68	-	+4.46	−31.21	0.885
MN15//PBE0	LTS/Argy-LPSC	−22.76	-	+3.96	−18.79	0.402
PBE0	LTS_{even}/Argy-Li_2S	−22.73	+12.14	+3.58	−19.15	1.18
MN15//PBE0	LTS_{even}/Argy-Li_2S	−32.02	-	+3.82	−28.20	0.82
PBE0	LTS_{odd}/Argy-Li_2S	−23.95	+11.95	+3.32	−20.63	1.31
MN15//PBE0	LTS_{odd}/Argy-Li_2S	−33.28	-	+3.83	−29.45	1.01
PBE0	LTS_{over}/Argy-Li_2S	−23.45	+5.43	+3.26	−20.19	2.04
MN15//PBE0	LTS_{over}/Argy-Li_2S	−34.94	-	+4.37	−30.57	1.54

We begin by examining interfaces involving pristine LTS. Figure 4 clearly shows the formation of chemical bonds between the subunits, resulting in noticeable deformations in the adjacent layers near the interface. The average bond lengths at the interface for Ti–S (2.34–2.72 Å) and Li–S (2.42–2.53 Å) bonds fall within expected ranges and are similar to those observed on the pristine LTS surface. Nevertheless, in LTS/Argy-LPSC, there are fewer types of bonds (3 types: Li(LTS)–S(PS_4), S(LTS)–Li(Li_2S), and Ti(LTS)–S(PS_4)) compared to LTS/Argy-Li_2S (5 types: Ti(LTS)–S(Li_2S), Ti(LTS)–Li(Li_2S), S(LTS)–Li(Li_2S), Li(LTS)–S(Li_2S), and S(LTS)–Li(Li_2S)). This difference can explain the larger stabilization of LTS/Argy, $E^c_{adh} = -21.62$ meVÅ^{-2} (PBE0), nearly four times higher than the value computed for LTS/Argy-LPSC, $E^c_{adh} = -6.12$ meVÅ^{-2}, due to the superior chemical compatibility of the Li_2S termination of Argyrodite with LTS in LTS/Argy-Li_2S compared to the PS_4 termination in LTS/Argy-LPSC.

Additionally, the charge density difference maps between the interfaces and pristine subunits (Figure 5) reveal depletion or accumulation of charge in Li–S and Ti–S bonds, further confirming the formation of new bonds and rearrangement of existing ones by highlighting the localization of the electron density between interface atoms. In the LTS/Argy-Li_2S heterostructure, these changes primarily affect the atomic layer adjacent to the interface, with minimal alteration observed in the rest of the system. In contrast, in the LTS/Argy-LPSC heterostructure, these effects extend through to more internal layers of each subunit, indicating a more extensive bond adjustment potentially at the expense of the energy gain from junction formation.

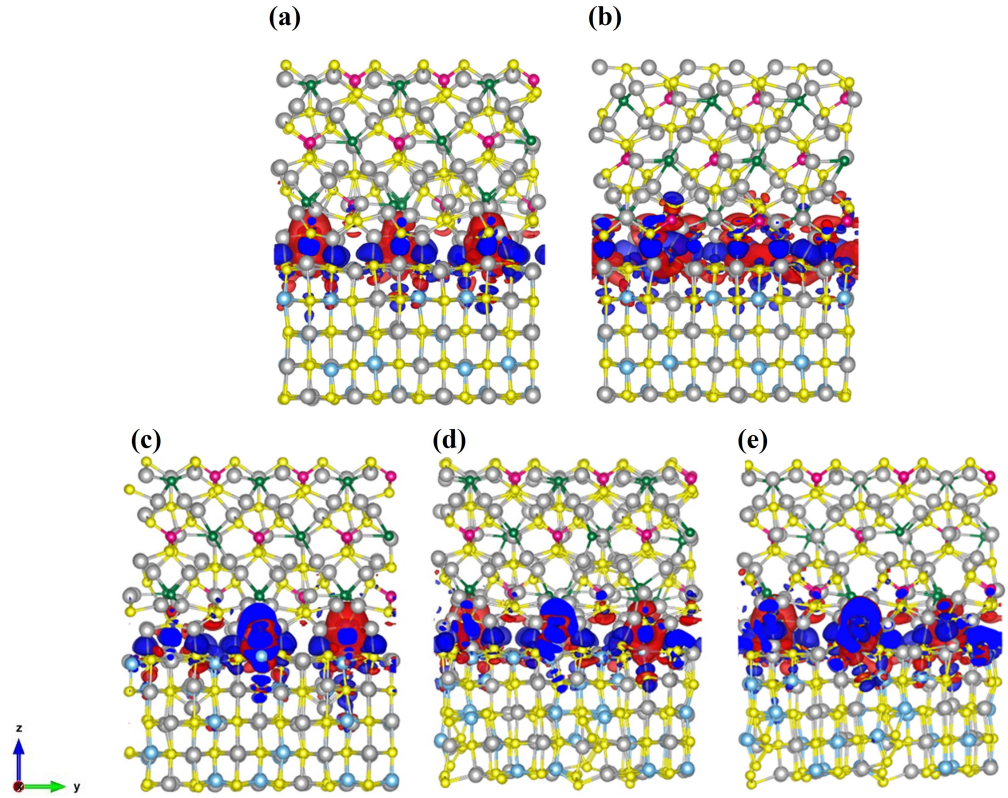

Figure 5. Charge density difference between interface and the pristine sub-units of (**a**) LTS/Argy-Li_2S, (**b**) LTS/Argy-LPSC, (**c**) LTS_{over}/Argy-Li_2S, (**d**) LTS_{even}/Argy-Li_2S, and (**e**) LTS_{odd}/Argy-Li_2S. The isosurface corresponds to 0.001 e^-/$bhor^3$ with the charge accumulation (depletion) plotted in red (blue). The yellow, gray, light blue, green, and magenta spheres represent the sulfur, lithium, titanium, chlorine, and phosphorus atoms.

Since (001) Argy with Li_2S termination gives rise to a more stable interface, it will be used to build up heterostructures with delithiated and overlithiated LTS.

In order to simulate the interface stability with different Li content in LTS, the models for heterostructures involving delithiated LTS (LTS_{even}/Argy and LTS_{odd}/Argy) and overlithiated (LTS_{over}/Argy) were also constructed (see Figure 4). Given that LTS_{odd}, LTS_{even}, and LTS_{over} contain structural units with S–S bridges and an additional number of Li atoms, respectively, they exhibit a certain degree of cell expansion compared to pristine LTS. This expansion results in a significantly larger strain energy, as shown in Table 3.

Interfaces formed with delithiated and overlithiated (100) LTS surfaces exhibit adhesion energies similar to pristine (100) LTS: −19.15 meV $Å^{-2}$, −20.63 meV $Å^{-2}$, and −20.19 meV $Å^{-2}$, for LTS_{even}/Argy-Li_2S, LTS_{odd}/Argy-Li_2S, and LTS_{over}/Argy-Li_2S, respectively (see Table 3). This suggests that the bonding between LTS and Argyrodite is not significantly affected by the lithium content. The primary characteristics of these interfaces closely resemble those computed for pristine LTS, as indicated by Table 3 and the comparison of panel (a) with panels (c–e) in Figures 4 and 5. In both delithiated and overlithiated structures, electron holes or excess electrons are well localized within the LTS substrate. This localization results in partial oxidation of S^{2-} and reduction of Ti^{4+} to Ti^{3+} without any electron transfer between the two subunits, as shown by the spin-polarized maps reported in Figure 6.

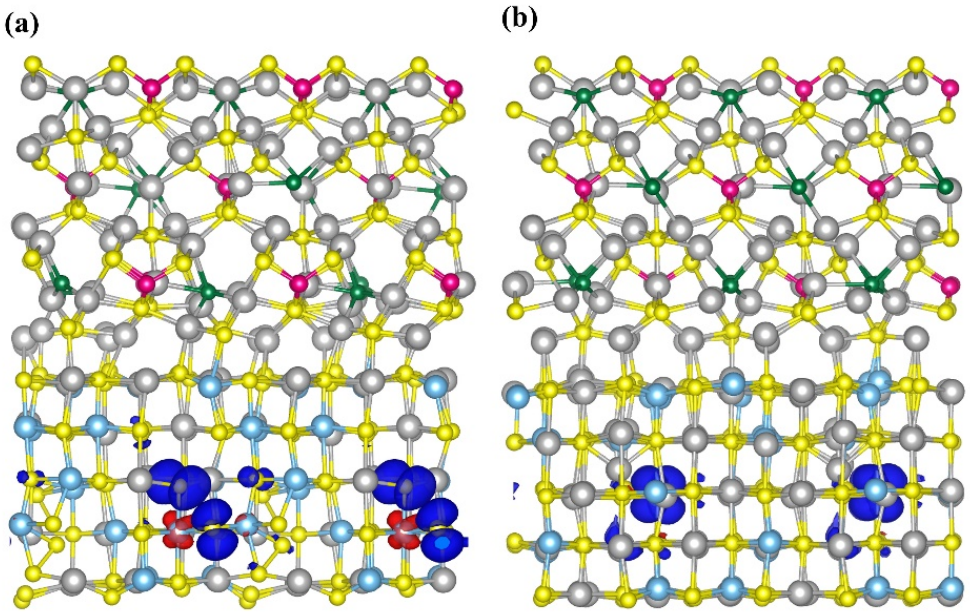

Figure 6. Spin density for the (**a**) LTS_{odd}/Argy-Li_2S and (**b**) LTS_{over}/Argy-Li_2S interface. The isosurface corresponds to 0.001 e^-/$bohr^{-3}$. The yellow, gray, light blue, green, and magenta spheres represent the sulfur, lithium, titanium, chlorine, and phosphorus atoms.

The main difference from the pristine system lies in the increased strain observed in both delithiated and overlithiated interfaces, as detailed in Table 3. This increased strain results from the removal and addition of lithium atoms, leading to structural expansion, as previously discussed and highlighted in [7]. Such findings indicate potential mechanical issues, as electrochemical bias can lead to high mechanical stress and interface breakdown. This issue can be addressed experimentally by adjusting the applied pressure to achieve a stable interface. This strategy is currently applied for Li metal and oxide sulfur interface, see Ref. [28].

To analyze the dependence of the computed heterostructure characteristics with the employed level of theory, E^c_{adh} values were also computed at the MN15//PBE0 level, identifying the same trend shown by PBE0 values, even if MN15 energy values are significantly larger (they range from -18 meV $Å^{-2}$ to -31 meV $Å^{-2}$, see Table 3). The MN15 functional may offer a more accurate description of energetics, particularly in scenarios where noncovalent interactions play a crucial role, such as in interfaces involving metals and notably large anions like S^{2-}. The overall charge transfers (CT) at the interface follow a similar trend to the adhesion energy. Our previous study [9] has established a correlation between charge transfer, interface bond formation, and adhesion strength. The values obtained in this study reaffirm this correlation and emphasize the influence of bond polarization on the attractive forces between surfaces, which plays a crucial role in stabilizing the heterostructure.

The analysis of the electronic properties was carried out using PDOS shown in Figure S2. The TVB of all interfaces is dominated by Li and S states from both LTS and Argy, overlapping in the region $-6/-9$ eV, indicating the formation of Li-S bonds, while BCB level is mainly due to LTS states.

ΔE values (see Figure 3) estimated for the heterostructures are marginally modified with respect to the corresponding values derived by band alignment in the separated components: the TVB of Argyrodite and BCB of LTS that defined this energy difference are moderately shifted upon the interface formation. ΔE is 2.35 eV for LTS/Argy-Li_2S and slightly changes during delithiation and overlithiation. In the delithiated system, ΔE = 2.14 eV and 1.80 eV for LTS_{even}/Argy- Li_2S and LTS_{odd}/Argy- Li_2S, respectively, and 2.09 eV in the overlithiated structure. While the ΔE values can only provide semi-quantitative information, it is interesting to note that the data provided for the explicit heterostructures shows less fluctuations with LTS lithium content than that for its separate

components, further suggesting the chemical resistance of Argyrodite towards oxidation under these conditions, even when in contact with Li-rich and Li-deficient cathode structures.

4. Conclusions

In this paper, interfaces between disordered cubic Li_2TiS_3 and Argyrodite Li_6PS_5Cl were investigated. The study of this system is of great interest since these two materials can be employed for all-solid-state lithium-ion batteries applications. The system was studied by means of periodic DFT calculations for the simulation of the surfaces and interfaces to comprehend the affinity between these two materials.

The (001) Li_6PS_5Cl surface, derived from our previous work [9], was chosen due to the presence of an exposed L_2S passivating layer. The surfaces for Li_2TiS_3 were constructed based on optimized structures from our earlier studies [6,7]. The (100) surface of LTS, identified as the most stable, was selected to reproduce the surface of a cathode made from this material. To broaden the scope of this study, the LTS was simulated at three different states of lithiation—pristine, overlithiated, and delithiated Li_2TiS_3—corresponding to the equilibrium, charged, and discharged states, respectively. The three LTS states were then paired with the Li_2S-terminated Li_6PS_5Cl surface, achieving optimal chemical compatibility between the two systems, according to computing chemical, electronic, and mechanical properties.

From the energetic point of view, lithium removal (delithiated) or addition (overlithiated) does not affect interface stability, even if the larger strain identified in delithiated and overlithiated structures could lead to mechanical issues. To evaluate chemical stability, we refer to the energy difference (ΔE) between the valence band of Argyrodite and the conduction band of LTS. In pristine, delithiated, and overlithiated conditions, the ΔE values indicate that electrolyte oxidation is not a spontaneous process. However, in this work, we assumed that the energy level can be used as descriptor for the electrochemical potential driving the electrolyte oxidation at the interface, but we would underline that they cannot correspond to real electrochemical reactions and have to be employed mindfully, see ref. [29].

Although the models presented in this work for LTS/Argy interfaces do not explicitly account for operational conditions that could affect long-term stability, such as prolonged electrochemical potential and mechanical stress, we have extracted significant data that shed light on the stability of LTS/Argy heterostructures with respect to lithium content by examining the chemical stability of the heterojunction under ideal conditions. Our findings demonstrate that Argyrodite has the potential to be effectively coupled with the LTS cathode material within the scope of our models, and this interface remains stable under various lithiation conditions. The goal of our work was to provide guidance to experimental teams, suggesting that these two materials can be successfully coupled. The similar sulfur-based chemistry of the materials indicates that chemical and electrochemical compatibility could theoretically be achieved.

Supplementary Materials: The following supporting information can be downloaded at: https://www.mdpi.com/article/10.3390/batteries10100351/s1. Figure S1: Projected density of states (PDOS) for the pristine surfaces. Figure S2: Projected density of states (PDOS) of all interfaces. Figure S3: Wulff crystal shape for the ideal and modified LTS.

Author Contributions: Conceptualization, R.R. and A.M.F.; data curation, R.R., N.L.M., F.S., E.A., M.D. and A.M.F.; writing—original draft preparation, R.R., N.L.M. and A.M.F.; writing—review and editing, R.R., M.F.S., E.A., F.S., N.L.M., N.L.P., M.D. and A.M.F.; supervision M.F.S. and A.M.F. All authors have read and agreed to the published version of the manuscript.

Funding: This research received no external funding.

Data Availability Statement: The original contributions presented in the study are included in the article and Supplementary Materials, further inquiries can be directed to the corresponding author.

Acknowledgments: The access to the CINECA National Supercomputing Service for HPC facilities (ISCRA B project HP10BYBKEM is kindly acknowledged. We acknowledge support from Project CH4.0 under the MUR program "Dipartimenti di Eccellenza 2023–2027" (CUP: D13C22003520001).

Conflicts of Interest: Authors Riccardo Rocca and Nello Li Pira were employed by the company Centro Ricerche FIAT S.C.p.A. The remaining authors declare that the research was conducted in the absence of any commercial or financial relationships that could be construed as a potential conflict of interest.

References

1. Sakuda, A.; Takeuchi, T.; Shikano, M.; Ohara, K.; Fukuda, K.; Uchimoto, Y.; Ogumi, Z.; Kobayashi, H.; Sakaebe, H. Development of Li_2TiS_3–Li_3NbS_4 by a mechanochemical process. *J. Ceram. Soc. Jpn.* **2017**, *125*, 268–271. [CrossRef]
2. Grimaud, A.; Hong, W.T.; Shao-Horn, Y.; Tarascon, J.-M. Anionic redox processes for electrochemical devices. *Nat. Mater.* **2016**, *15*, 121–126. [CrossRef] [PubMed]
3. Sakuda, A.; Ohara, K.; Kawaguchi, T.; Fukuda, K.; Nakanishi, K.; Arai, H.; Uchimoto, Y.; Ohta, T.; Matsubara, E.; Ogumi, Z.; et al. A Reversible Rocksalt to Amorphous Phase Transition Involving Anion Redox. *Sci. Rep.* **2018**, *8*, 15086. [CrossRef] [PubMed]
4. Sakuda, A.; Takeuchi, T.; Okamura, K.; Kobayashi, H.; Sakaebe, H.; Tatsumi, K.; Ogumi, Z. Rock-salt-type lithium metal sulphides as novel positive-electrode materials. *Sci. Rep.* **2015**, *4*, 4883. [CrossRef]
5. Sakuda, A.; Kuratani, K.; Takeuchi, T.; Kiuchi, H.; Kawaguchi, T.; Shikano, M.; Sakaebe, H.; Kobayashi, H. Cubic Rocksalt Li_2SnS_3 and a Solid Solution with Li_3NbS_4 Prepared by Mechanochemical Synthesis. *Electrochemistry* **2017**, *85*, 580–584. [CrossRef]
6. Rocca, R.; Sgroi, M.F.; Camino, B.; D'Amore, M.; Ferrari, A.M. Disordered Rock-Salt Type Li_2TiS_3 as Novel Cathode for LIBs: A Computational Point of View. *Nanomaterials* **2022**, *12*, 1832. [CrossRef]
7. Rocca, R.; Sgroi, M.F.; D'amore, M.; Li Pira, N.; Ferrari, A.M. Computational Understanding of Delithiation, Overlithiation, and Transport Properties in Disordered Cubic Rock-Salt Type Li_2TiS_3. *Nanomaterials* **2023**, *13*, 3013. [CrossRef]
8. Le Mong, A.; Ahn, Y.; Puttaswamy, R.; Kim, D. Pore filled solid electrolytes with high ionic conduction and electrochemical stability for lithium sulfur battery. *Energy Mater.* **2023**, *3*, 300035. [CrossRef]
9. D'Amore, M.; Daga, L.E.; Rocca, R.; Sgroi, M.F.; Marana, N.L.; Casassa, S.M.; Maschio, L.; Ferrari, A.M. From symmetry breaking in the bulk to phase transitions at the surface: A quantum-mechanical exploration of Li_6PS_5 Cl argyrodite superionic conductor. *Phys. Chem. Chem. Phys.* **2022**, *24*, 22978–22986. [CrossRef]
10. Deiseroth, H.; Kong, S.; Eckert, H.; Vannahme, J.; Reiner, C.; Zaiß, T.; Schlosser, M. Li_6PS_5X: A Class of Crystalline Li-Rich Solids with an Unusually High Li^+ Mobility. *Angew. Chem. Int. Ed.* **2008**, *47*, 755–758. [CrossRef]
11. Yu, C.; Ganapathy, S.; Hageman, J.; Van Eijck, L.; Van Eck, E.R.H.; Zhang, L.; Schwietert, T.; Basak, S.; Kelder, E.M.; Wagemaker, M. Facile Synthesis toward the Optimal Structure-Conductivity Characteristics of the Argyrodite Li_6PS_5Cl Solid-State Electrolyte. *ACS Appl. Mater. Interfaces* **2018**, *10*, 33296–33306. [CrossRef] [PubMed]
12. Tron, A.; Orue, A.; López-Aranguren, P.; Beutl, A. Critical Current Density Measurements of Argyrodite Li_6PS_5Cl Solid Electrolyte at Ambient Pressure. *J. Electrochem. Soc.* **2023**, *170*, 100525. [CrossRef]
13. Celasun, Y.; Colin, J.-F.; Martinet, S.; Benayad, A.; Peralta, D. Lithium-Rich Rock Salt Type Sulfides-Selenides ($Li_2TiSe_xS_{3-x}$): High Energy Cathode Materials for Lithium-Ion Batteries. *Materials* **2022**, *15*, 3037. [CrossRef] [PubMed]
14. Erba, A.; Desmarais, J.K.; Casassa, S.; Civalleri, B.; Donà, L.; Bush, I.J.; Searle, B.; Maschio, L.; Edith-Daga, L.; Cossard, A.; et al. CRYSTAL23: A Program for Computational Solid State Physics and Chemistry. *J. Chem. Theory Comput.* **2023**, *19*, 6891–6932. [CrossRef]
15. Perdew, J.P.; Wang, Y. Accurate and simple analytic representation of the electron-gas correlation energy. *Phys. Rev. B* **1992**, *45*, 13244–13249. [CrossRef]
16. Adamo, C.; Barone, V. Toward reliable density functional methods without adjustable parameters: The PBE0 model. *J. Chem. Phys.* **1999**, *110*, 6158–6170. [CrossRef]
17. Ojamäe, L.; Hermansson, K.; Pisani, C.; Causà, M.; Roetti, C. Structural, vibrational and electronic properties of a crystalline hydrate from ab initio periodic Hartree–Fock calculations. *Acta Crystallogr. B* **1994**, *50*, 268–279. [CrossRef]
18. Lichanot, A.; Aprà, E.; Dovesi, R. Quantum Mechnical Hartree-Fock Study of the Elastic Properties of Li_2S and Na_2S. *Phys. Status Solidi B* **1993**, *177*, 157–163. [CrossRef]
19. Zicovich-Wilson, C.M.; Bert, A.; Roetti, C.; Dovesi, R.; Saunders, V.R. Characterization of the electronic structure of crystalline compounds through their localized Wannier functions. *J. Chem. Phys.* **2002**, *116*, 1120–1127. [CrossRef]
20. Hay, P.J.; Wadt, W.R. Ab initio effective core potentials for molecular calculations. Potentials for K to Au including the outermost core orbitals. *J. Chem. Phys.* **1985**, *82*, 299–310. [CrossRef]
21. Marana, N.L.; Silveri, F.; de Oliveira Gomes, E.; Donà, L.; D'Amore, M.; Ascrizzi, E.; Sgroi, M.F.; Maschio, L.; Ferrari, A.M. A computational study of the negative LiIn modified anode and its interaction with β-Li_3PS_4 solid–electrolyte for battery applications. *Phys. Chem. Chem. Phys.* **2024**, *26*, 15648–15656. [CrossRef] [PubMed]
22. Sorrentino, A.L.; Serrano, G.; Poggini, L.; Cortigiani, B.; El-Kelany, K.E.; D'Amore, M.; Ferrari, A.M.; Atrei, A.; Caneschi, A.; Sessoli, R.; et al. Quasi-Hexagonal to Lepidocrocite-like Transition in TiO_2 Ultrathin Films on Cu(001). *J. Phys. Chem. C* **2021**, *125*, 10621–10630. [CrossRef]

23. Yu, H.S.; He, X.; Li, S.L.; Truhlar, D.G. MN15: A Kohn–Sham global-hybrid exchange–correlation density functional with broad accuracy for multi-reference and single-reference systems and noncovalent interactions. *Chem. Sci.* **2016**, *7*, 5032–5051. [CrossRef] [PubMed]
24. Van Duijneveldt, F.B.; Van Duijneveldt-van De Rijdt, J.G.C.M.; Van Lenthe, J.H. State of the Art in Counterpoise Theory. *Chem. Rev.* **1994**, *94*, 1873–1885. [CrossRef]
25. Yu, C.; Zhao, F.; Luo, J.; Zhang, L.; Sun, X. Recent development of lithium argyrodite solid-state electrolytes for solid-state batteries: Synthesis, structure, stability and dynamics. *Nano Energy* **2021**, *83*, 105858. [CrossRef]
26. Marana, N.L.; Casassa, S.; Sgroi, M.F.; Maschio, L.; Silveri, F.; D'Amore, M.; Ferrari, A.M. Stability and Formation of the Li_3PS_4/Li, Li_3PS_4/Li_2S, and Li_2S/Li Interfaces: A Theoretical Study. *Langmuir* **2023**, *39*, 18797–18806. [CrossRef]
27. D'Amore, M.; Yang, M.Y.; Das, T.; Ferrari, A.M.; Kim, M.M.; Rocca, R.; Sgroi, M.; Fortunelli, A.; Goddard, W.A.I. Understanding Ionic Diffusion Mechanisms in Li_2S Coatings for Solid-State Batteries: Development of a Tailored Reactive Force Field for Multiscale Simulations. *J. Phys. Chem. C* **2023**, *127*, 22880–22888. [CrossRef]
28. Yang, M.; Liu, Y.; Nolan, A.M.; Mo, Y. Interfacial Atomistic Mechanisms of Lithium Metal Stripping and Plating in Solid-State Batteries. *Adv. Mater.* **2021**, *33*, 2008081. [CrossRef]
29. Peljo, P.; Girault, H.H. Electrochemical potential window of battery electrolytes: The HOMO–LUMO misconception. *Energy Environ. Sci* **2018**, *11*, 2306–2309. [CrossRef]